EARTH SURFACE PROCESSES AND LANDFORMS
Earth Surf. Process. Landforms **35**, 1516–1534 (2010)

Published online 28 June 2010 in Wiley Online Library
(wileyonlinelibrary.com) DOI: 10.1002/esp.1992

The topographic imprint of a transient climate episode: the western Andean flank between 15·5° and 41·5°S†

K. Rehak,[1,2]* B. Bookhagen,[3,4] M. R. Strecker[1] and H. P. Echtler[1,5]
[1] Institut für Geowissenschaften, Universität Potsdam, Potsdam, Germany
[2] Helmholtz Association, Berlin, Germany
[3] Stanford University, Department of Geological and Environmental Sciences, California, USA
[4] Department of Geography, University of California at Santa Barbara, California, USA
[5] GFZ Potsdam, Department Geodäsie und Fernerkundung, Potsdam, Germany

Received 27 May 2008; Revised 27 November 2009; Accepted 14 December 2009

*Correspondence to: K. Rehak, Helmholtz Association, Berlin, Germany. E-mail: k.rehak@email.de
†Correction added on 2 September, after first online publication. The location information has been added to part D of Figure 3

ESPL
Earth Surface Processes and Landforms

ABSTRACT: Mountain-range topography is determined by the complex interplay between tectonics and climate. However, often it is not clear to what extent climate forces topographic evolution and how past climatic episodes are reflected in present-day relief.

The Andes are a tectonically active mountain belt encompassing various climatic zones with pronounced differences in rainfall, erosion, and glacier extent under similar plate-boundary conditions. In the central to south-western Andes, climatic zones range from hyperarid desert with mean annual rainfall of 5 mm/a (22·5°S) to year-round humidity with 2500 mm/a (40°S). The Andes thus provide a unique setting for investigating the relationship between tectonics, climate, and topography.

We present an analysis of 120 catchments along the western Andean watersheds between 15·5° and 41·5°S, which is based on SRTMV3-90m data and new medium-resolution rainfall, tropical rainfall measurement mission (TRMM) dataset. For each basin, we extracted geometry, relief, and climate parameters to test whether Andean topography shows a climatic imprint and to analyze how climate influences relief.

Our data document that elevation and relief decrease with increasing rainfall and descending snowline elevation. Furthermore, we show that local relief reaches high values of 750 m in a zone between 28°S to 35°S. During Pleistocene glacial stages this region was affected by the northward shifting southern hemisphere Westerlies, which provided moisture for valley-glacier formation and extended glacial coverage as well as glacial erosion. In contrast, the southern regions between 35°S to 40°S receive higher rainfall and have a lower local relief of 200 m, probably related to an increased drainage density. We distinguish two different, climatically-controlled mechanisms shaping topography: (1) fluvial erosion by prolonged channel-hillslope coupling, which smoothes relief, and (2) erosion by valley glaciers that generates relief. Finally, Our results suggests that the catchment-scale relief of the Andes between 28°S to 35°S is characterized by a pronounced transient component reflecting past climatic conditions. Copyright © 2010 John Wiley & Sons, Ltd.

KEYWORDS: drainage basins; topography; transient landscape; climate; erosion

Introduction

Landscapes are sensitive recorders of surface processes driven by climate and tectonics. The topographic signature of a landscape can thus provide important insights into the complex interaction between climatic and tectonic processes. Climate undoubtedly plays a major role in creating relief and shaping topography (e.g., Büdel, 1982; Molnar and England, 1990). Modeling studies suggest that increased precipitation might cause a reduction of mountain-range topography and strongly influences drainage-basin morphology (Tucker and Slingerland, 1997; Whipple and Tucker, 1999; Willett, 1999; Roe *et al.*, 2003). Roe *et al.* (2003) suggest that in rainfall-dominated environments mountain ranges can be lowered by more than half due to enhanced rainfall. Also river-profile concavity (e.g., Roe *et al.*, 2002; Zaprowski *et al.*, 2005) and mountain-range widths (Whipple and Meade, 2006) appear to be coupled to rainfall. It has been suggested that a reduction of topography and concavity of river profiles could be controlled by an increase in drainage density, which might lower hillslope, tributary, and trunk channel relief, as well as threshold hillslope angles (Tucker and Bras, 1998; Whipple *et al.*, 1999; Reiners *et al.*, 2003; Gabet *et al.*, 2004). These inferred feedbacks are generally corroborated by field studies (Montgomery *et al.*, 2001; Gabet *et al.*, 2004). For example, in the tectonically active Himalaya Gabet *et al.* (2004) document that a doubling of annual rainfall from 2000 to 4000 mm results in a 33% decrease in total relief.

Conversely, glacial erosion appears to be one of the main relief-generating processes focusing the removal of material near the peaks, and thereby maintaining steep topography

above the equilibrium-line altitude (ELA) and limiting range height (Hallet *et al.*, 1996; Brozovic *et al.*, 1997; Small and Anderson, 1998; Whipple *et al.*, 1999; Montgomery *et al.*, 2001; Tomkin and Braun, 2002; Mitchell and Montgomery, 2006). However, the role of climate-induced relief production has been challenged and it has been argued that tectonically active mountain belts are already characterized by threshold relief (Whipple *et al.*, 1999; Montgomery and Brandon, 2002). The controversies emphasize that fundamental key questions concerning the interactions between topography and climate have not been fully answered yet. In this context, it is important to investigate the influence of climate on mountain-range morphology and topography. In addition to modeling efforts these interactions should be studied in real orogens.

A good starting point to analyze the imprint of climate on topography constitutes the comparison of drainage basins located in different climatic settings, where all other dependent variables, such as lithology and general tectonic boundary conditions, are similar. Ideally, the overall characteristics of climate should have been sustained over longer time scales in a well constrained tectonic system. These requirements are reasonably fulfilled along the west coast of South America. Indeed, the Andes provide a unique setting for investigating the relationship between climate and topography. More than 7000 km long, the Andes are a meridionally oriented, tectonically active orogen spanning large climatic gradients from hyper-arid to humid, controlled by stable, hemisphere-scale atmospheric circulation patterns that persisted at least during Quaternary and possibly over the Neogene (Schwerdtfeger, 1976; Bice *et al.*, 2000; Haselton *et al.*, 2002; Hartley and Chong, 2002).

We conducted a detailed analysis of the western Andean flank between 15·5°S and 41·5°S. Using new TRMM product 3B42 (Huffmann *et al.*, 2007) with ~25 km × 25 km spatial resolution and the topographic SRTMV3-90-m data, we extracted 19 geometry, relief, and climate parameters for 120 drainage basins. Therewith, we address the following questions: (1) How does rainfall in this environment affect the topography of drainage basins and why? (2) What is the impact of glaciations on the topography of drainage basins? (3) Does climate also influence basin morphometry? Based on the potential interactions between climate and topography we expect to see a clear imprint of the different prevailing climatic zones on the relief of the western Andean flank. Additionally, landscapes might not only reflect prevailing climatic conditions, but could also show the imprint of past climatic episodes. Our data expands the rainfall range of other studies significantly (e.g. Zaprowski *et al.*, 2005) and enables us to better understand the climatic controls of relief generation in mountain ranges, especially with regard to transience in landscapes and the role of rainfall on relief evolution.

Regional Setting

Geologic setting

The Andean margin is characterized by the subduction of the Nazca plate beneath the South American continent at a rate of approximately 65 to 85 mm/a (Demets *et al.*, 1994; Somoza, 1998; Angermann *et al.*, 1999). The pre-Andean basement evolved during a period of already east-directed subduction (Pankhurst and Hervé, 2007). The basement rocks are subdivided into crustal segments, comprising exotic terranes, such as the Precordillera Terrane, as well as late Paleozoic to early Mesozoic igneous and metamorphic rocks, batholiths, and accreted marine sequences that constitute arc-forearc complexes (Hervé, 1988; Mpodozis and Ramos, 1989; Parada, 1990; Glodny *et al.*, 2005; Hervé *et al.*, 2007; Pankhurst and Hervé, 2007). This basement was strongly overprinted by subduction-related tectonic and magmatic processes, which have operated since the Jurassic period (Mpodozis and Ramos, 1989; Allmendinger *et al.*, 1997).

The recent phase of contraction and shortening that initiated the uplift of the Andes was accompanied by extensive arc activity starting in the Eocene in the Central Andes; in the Northern Patagonian Andes these processes began in the early Miocene (Allmendinger *et al.*, 1990; Jordan, 1993; Kley and Monaldi, 1998; Oncken *et al.*, 2006). Total shortening decreases southward from ~ 300 km in the Central Andes to only ~ 15 km in the Northern Patagonian Andes (Isacks, 1988; Allmendinger *et al.*, 1990; Diraison *et al.*, 1998; Kley *et al.*, 1999; Gregory-Wodzicki, 2000; Oncken *et al.*, 2006; Vietor and Echtler, 2006; Glodny *et al.*, 2008) (Figure 1). Global positioning system (GPS) measurements corroborate this long-term pattern and document higher shortening rates in the Central Andes (Dewey and Lamb, 1992; Klotz *et al.*, 2001; Brooks *et al.*, 2003).

Based on shortening rates and tectonic activity, the Central to Southern Andes can be subdivided into four tectonic provinces (Figure 1). (1) The central part from 14°S to 27°S comprises the Coastal Cordillera, the Central Depression, the Precordillera and the Main Cordillera with the internally drained intraorogenic plateaus of the Altiplano and Puna that display mean elevations of 3700 m. This sector displays pronounced crustal shortening in the Main Cordillera and the Subandean Ranges (Mpodozis and Ramos, 1989). (2) The region between 27°S and 33°S is characterized by flat-slab subduction and a related absence of late Neogene to Quaternary volcanism and a Central Depression (Jordan *et al.*, 1983; Mpodozis and Ramos, 1989; Kay and Mpodozis, 2002; Ramos *et al.*, 2002). However, this region comprises the broken-foreland province of the Sierras Pampeanas that experiences active deformation and destructive earthquakes (Jordan and Allmendinger, 1986; Allmendinger *et al.*, 1990). (3) South of 31°S, total shortening is significantly reduced and south of 37° shortening has stopped at the end of the Miocene (Vietor and Echtler, 2006). South of 33°S the western onshore margin shows a pronounced morphotectonic segmentation integrating the forearc Coastal Cordillera, the Central Depression, and the Main Cordillera (Muñoz *et al.*, 2000). (4) South of ~37°S the Main Cordillera is called Patagonian Cordillera. Here, deformation is partitioned in intra-arc strike-slip tectonics along the Liquiñe-Ofqui fault zone and thrust faulting (Cembrano *et al.*, 2000; Thomson, 2002; Rosenau *et al.*, 2006).

Surface-uplift rates in the Main Cordillera are poorly constrained and only few studies provide information (Figure 1) (Farias *et al.*, 2005; Charrier *et al.*, 2007; Schildgen *et al.*, 2007). Therefore, we additionally consider Neogene uplift rates derived in the forearc along the coast. They vary between 0·2 and 2 mm/a and are relatively similar along the margin, except a patch of faster uplift in the region offshore the Arauco peninsula at ~37°S. This is a locally restricted forearc phenomenon and controlled by local high-angle reverse faults (Kaizuka *et al.*, 1973; Radtke, 1989; Atwater *et al.*, 1992; Nelson and Manley, 1992; Ortlieb *et al.*, 1996a; Ortlieb *et al.*, 1996b; Marquardt *et al.*, 2004; Le Roux *et al.*, 2005; Melnick *et al.*, 2006; Pino and Navarro, 2005; Bookhagen *et al.*, 2006; Le Roux *et al.*, 2006; Rehak *et al.*, 2008; Melnick *et al.*, 2009; Rehak *et al.*, in press) (Figure 1).

Climatic setting

From 15°S to 42°S the western flank of the Andes spans various climatic zones and rainfall regimes from the

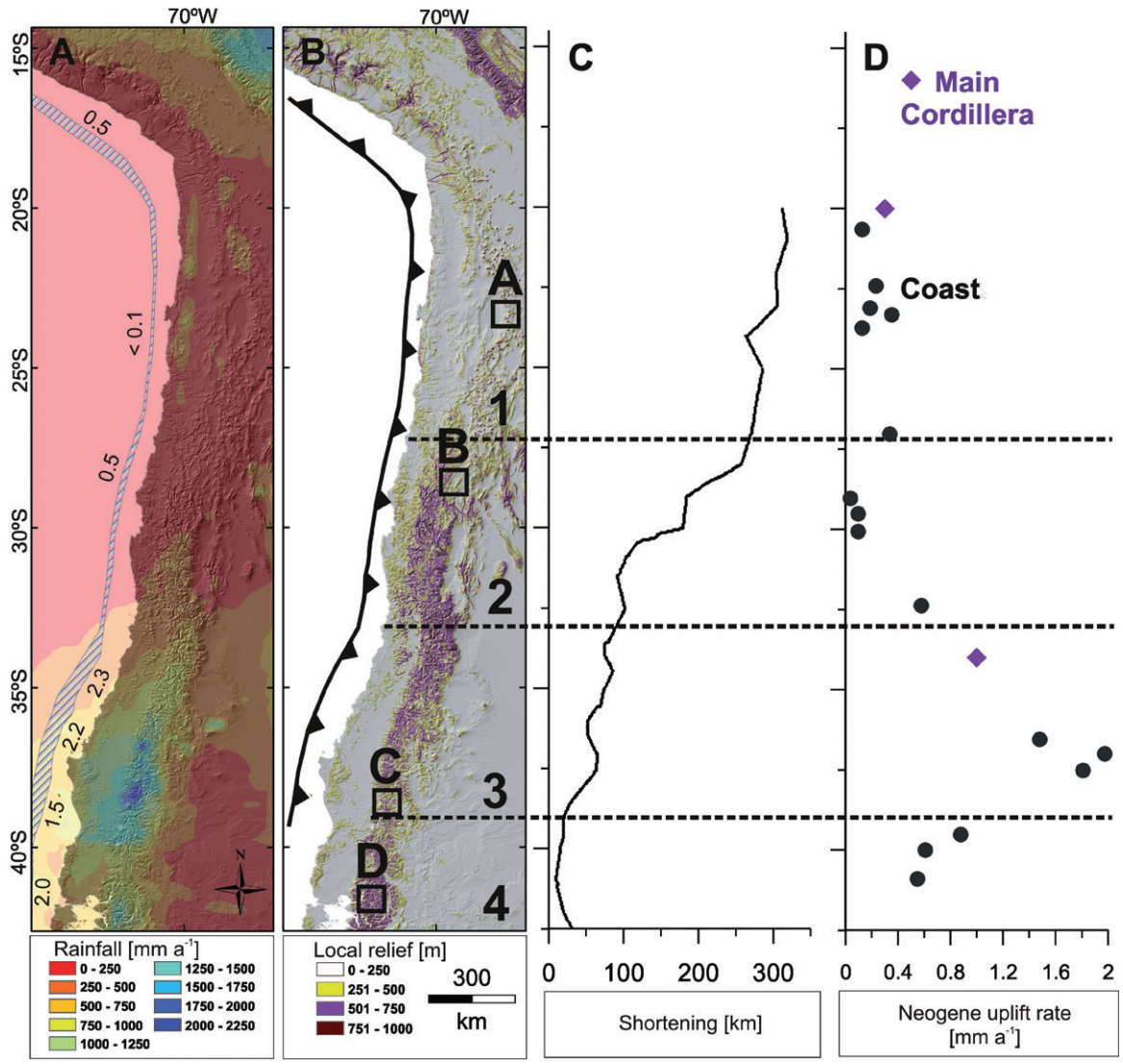

Figure 1. (A) Drainage basins analyzed with TRMM-rainfall data (Huffman *et al.*, 2007). Numbers indicate trench-fill thickness in kilometers (Bangs and Cande, 1997). Note the rainfall increase south of ~32°S and the rainfall maximum between 35°S to 40°S. (B) Local relief map calculated over a radius of 4·5 km with tectonic segments (Mpodozis and Ramos, 1989). Squares marked with A, B, C, and D outline the locations of the Landsat TM images in Figure 4. Segment 1 exhibits high crustal shortening comprising the plateau regions. Segment 2 is a flat-slab segment with active deformation in the Main Cordillera, but no Quaternary volcanism. Segment 3 is characterized by low shortening and minimal foreland deformation, however, high uplift rates in the forearc. Segment 4 also shows low shortening and the deformation expresses a dominant strike-slip component. Note the high relief areas between 30°S to 35°S and south of 40°S as well as the coincidence of the maximum rainfall and the lower local relief between 35°S to 40°S. (C) Total shortening along the south-central Andean margin (Vietor and Echtler, 2006). See the decrease in shortening at ~29°S. (D) Neogene uplift rates mostly derived from the forearc region (Kaizuka *et al.*, 1973; Radtke, 1989; Atwater *et al.*, 1992; Nelson and Manley, 1992; Ortlieb *et al.*, 1996a; Ortlieb *et al.*, 1996b; Marquardt *et al.*, 2004; Le Roux *et al.*, 2005; Melnick *et al.*, 2006; Pino and Navarro, 2005; Bookhagen *et al.*, 2006; Le Roux *et al.*, 2006) and from the Main Cordillera (Farias *et al.*, 2005; Charrier *et al.*, 2007; Schildgen *et al.*, 2007). This figure is available in colour online at wileyonlinelibrary.com

hyper-arid subtropical Atacama Desert with year-round aridity in the north and semi-arid environments with few months of winter rain in the central part to year-round humid regions in the south (Figure 1). Mean annual precipitation increases from zero in the core of the Atacama desert at 22°S to about 3500 mm/a on the windward western side of the Andes at 41°S (e.g. Kummerow *et al.*, 2000, New *et al.*, 2002, Bookhagen and Strecker, 2008). In the north the prevailing humid trade winds and the low-level Andean Jet from the east and north-east are blocked by the Andean topography (Strecker *et al.*, 2007). Together with the upwelling cold water of the Humboldt Current this promotes hyper-aridity on the western flanks in the north (e.g., Hartley and Chong, 2002). In contrast, the Westerlies directly deliver moisture to the western flanks south of ~30°S. The equatorial position of the Pacific anticyclone enables these westerly frontal systems to penetrate northwards and carry moisture into the arid regions as far north as 30°S, occasionally during mid-winter even up to 27°S (e.g. Schwerdtfeger, 1976). Between 27°S and 30°S this frontal rain occurs between May and August accounting for 90% of the total annual rainfall with each month's precipitation normally originating from only one frontal passage (e.g. Schwerdtfeger, 1976). The largest precipitation gradient occurs between 30°S and 35°S, where precipitation rates increase by one order of magnitude from 300 to 3000 mm/a.

Superposed on annual periodic rainfall variation, the region around 28°S is subjected to episodic variations from arid to semi-arid conditions due to increased moisture transport from the south controlled by a northward shift of the Southern Westerlies during glacial periods (e.g. Scholl *et al.*, 1970; Heusser, 1989; Clapperton, 1993; Veit, 1996; Lamy *et al.*, 1998; Lamy *et al.*, 2000; Jenny *et al.*, 2002; Romero *et al.*,

2006; Hebbeln *et al.*, 2007). Less extensive shifts of the Westerlies have occurred on shorter timescales in the recent geologic past (Lamy *et al.*, 1999). North of 27°S the plateau regions also recieved higher precipitation during the Pleistocene caused by easterly moisture incursion (Garreaud *et al.*, 2003). Taken together, the present-day and past conditions define a broad climatic and geomorphic transition zone on the western flank of the orogen between 28°S to 35°S, which is characterized by annual and glacial-interglacial rainfall variations.

The climatic zonation of the study area is controlled by long-lived, hemisphere-scale circulation patterns. The hyperarid conditions in the Atacama Desert were probably established at least 10 to 15 Ma ago, the arid conditions may have already been established during the Cretaceous, explaining the extremely low geomorphic process rates in this region (Hartley, 2003; Dunai *et al.*, 2005; Nishiizumi *et al.*, 2005; Rech *et al.*, 2006). The general circulation patterns in the southern Central Andes have persisted during the Pleistocene and may have been established in Oligocene to Miocene time, which implies that the humid conditions in the south have been stable and controlled by the Southern Westerlies over a very long time span (Schwerdtfeger, 1976; Bice *et al.*, 2000; Haselton *et al.*, 2002; Blisniuk *et al.*, 2005). This is supported by the fact that the distribution of precipitation is mimicked by the thickness of sediment fill in the trench off South America, which document a significant increase of sediment thickness south of the Juan-Fernández Ridge and support the long-term stability of the general precipitation pattern along the western Andean margin (Bangs and Cande, 1997; Melnick and Echtler, 2006) (Figure 1).

South of 41°S drainage basins are not integrated and frequently change size due to glacial erosion by ice caps (M. Mardones, personal communication, 2006). Consequently, these basins were not included in our analysis. Between about 18°S and 28°S recent glaciers do not exist and the elevation of the modern perennial snowline as well as the lowest Pleistocene glacier extent lie well above 5000 m. Thus, they exceed the maximum elevation of the drainage basins (Rabassa and Clapperton, 1990; Ammann *et al.*, 2001) and these catchments have not been influenced by Pleistocene glaciations.

Methodology

Along the western Andean flank from 15·5°S near Arequipa (Peru) to 41·5°S to Chiloé Island (Chile) we extracted a total of 120 drainage basins, comprising 64 main catchments draining into the Pacific and 56 equally-sized sub-catchments with a mean drainage area of 1000 km^2. According to their location, the main catchments were grouped into forearc, Andean mountain front, and arc catchments (Figure 2). This enables us to detect scale effects and to distinguish between basins shaped by different geomorphic processes. Forearc catchments drain only the Coastal Cordillera and have not been affected by Quaternary glaciations. In contrast, mountain-front catchments also include the Central Depression and the Andean foothills, nevertheless they do not extend into the high Andes and have mostly not been glaciated during the Quaternary. Arc catchments extend from the Pacific to the principal Andean watershed. Sub-catchments are parts of the arc catchments and constitute the uppermost headwater basins along the Andean main drainage divide. All sub-catchments were extracted based on a similar contributing area of ~500 to 2000 km^2 in order to identify and exclude orographic and scale effects. For each basin and its trunk stream we calculated 19 variables describing geometry, relief, and climate. Our analysis is based on the new medium-resolution (~25 km × 25 km) rainfall dataset TRMM 3B42 averaged over eight years from 1998 to 2006 (e.g., Huffman *et al.*, 2007; Kummerow *et al.*, 2000) and topographic SRTMV3-90-m data (USGS, 2007).

The variables are defined and summarized in Table I. All variables were correlated in order to identify relationships between basin geometry, range relief, climate, river-profile concavity and hypsometric integral. Total basin relief is calculated as the difference between the absolute maximum and the absolute minimum elevation of a catchment (Figure 2). In contrast, local relief describes the relief range in circles with a certain radius averaged for each basin. We apply a radius of 4·5 km, which assures the incorporation of the characteristic bandwidth of local relief in our region (e.g. Champagnac *et al.*, 2007; Purves and Korup, 2007) (Figure 2). Modern annual snowline and lowest Pleistocene glacier extent are compiled from Schwerdtfeger (1976) and Rabassa and Clapperton (1990).

River profiles are often interpreted with respect to climatic conditions, fluvial processes, rock-uplift rates, and evolutionary stage (e.g. Strahler, 1952; Summerfield, 1991; Ohmori, 1993; Whipple and Tucker, 1999; Snyder *et al.*, 2000; Kirby and Whipple, 2001). The concavity of a river-profile can be expressed as a profile-concavity index (PCI) (e.g. Demoulin, 1998). This reduces the river profile to a single number and enables correlation with other variables. The PCI is an indicator for the general channel topography and calculated as the normalized area under the normalized distance-elevation curve of the river (Figure 2). A diagonal drawn from the source to the mouth would result in a value of 0·5; thus, profiles with a PCI > 0·5 reflect convex shapes. The PCI is similar to stream-profile concavity used by Zaprowski *et al.* (2005), who found that this index covaries with concavity, the regression slope in log slope – log area plots. These authors hence concluded that both values are effective measures of profile concavity. We do not identify rainfall variations along single longitudinal-river profiles in this study.

The hypsometric integral (HI) describes the distribution of elevations in a drainage basin and thus basin topography. The HI is calculated as the normalized area under a normalized area-elevation curve, following Strahler (1952) (Figure 2). It is interpreted as a reflection of the geomorphic evolutionary stage and the degree of tectonic activity affecting landscapes (Strahler, 1952; Summerfield, 1991; Ohmori, 1993). Mature landscapes without significant tectonic activity are characterized by low relief contrasts and hence low integrals, whereas young, actively uplifting and deeply incised areas display high integrals (e.g. Strahler, 1952). However, basins showing the same HI are probably much older in arid environments than in humid climates due to differences in rainfall and denudation rates. In contrast, two basins, which started to uplift at the same time and are situated in different climatic zones should exhibit significantly distinct HI-values. Hence, HI-values might not only reflect the age of landscapes, but also erosional processes.

The variables were correlated separately for all basin groups. In our interpretation, we will mainly focus on the key parameters relief, elevation, rainfall, and snowline that we identified to elucidate the interactions between climate and topography. The significance level for all correlations was set to the 95% confidence interval of a two tailed *t*-test. As a goodness-of-fit measure for the correlations and regressions we used the constant of regression (R^2).

Lithologies were determined by a geological map (Servicio Nacional de Geológía y Minería, 2003). They vary non-systematically along the active continental margin between

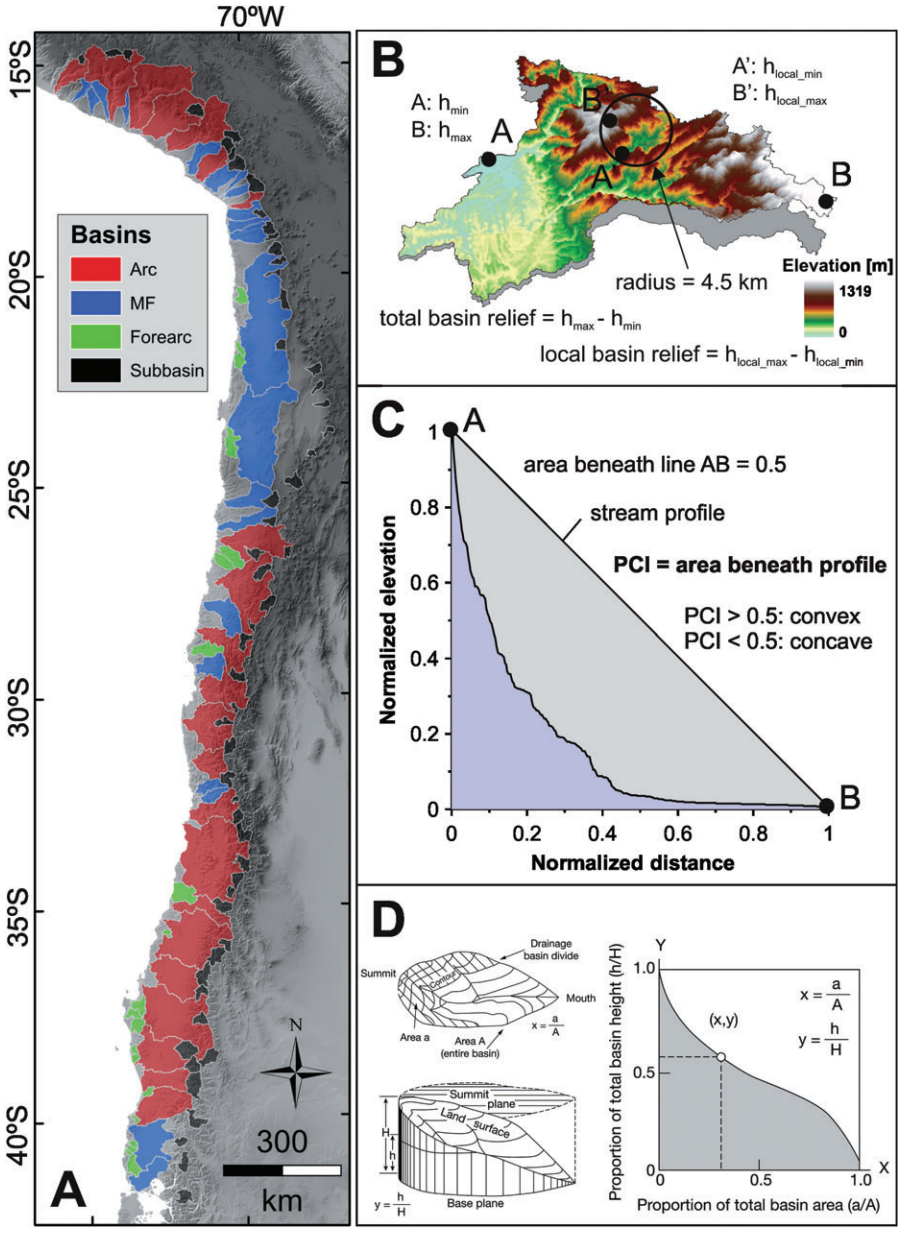

Figure 2. (A) Analyzed basins along the Andean margin. Arc catchments reach from the Pacific Ocean up to the principal Andean drainage divide, mountain-front catchments reach the Andean foothills. Forearc catchments drain only the Coastal Ranges. Sub-catchments are mostly part of the arc catchments and constitute headwater basins along the watershed. (B) Sample catchment demonstrating the calculation of total and local basin relief. (C) The PCI is an integral describing the area beneath a river-longitudinal profile. (D) Generation of the hypsometric curve and the related hypsometric integral defined as the area beneath the curve. This figure is available in colour online at wileyonlinelibrary.com

15°S and 40°S and do not correlate with climatic zonation. Data on surface-uplift rates in the Main Cordillera is very sparse. Thus, we have to rely on proxy indicators such as surface-uplift data from the forearc, the intensity of active deformation, and trench-normal shortening.

Results and Interpretation

The analysis of 120 drainage basins along the Central and Southern Andes shows evidence for a prominent imprint of climate on topography. Landsat TM images of typical headwater basins reveal the distinct character of local catchment relief in the different climatic zones (Figure 3). The northern basins in the hyper-arid part show a very low local relief. This landscape is virtually undissected and characterized by extremely low erosion rates <0·1 m/Ma (Nishiizumi *et al.*, 2005) resulting in the preservation of mid-Miocene relict surfaces (Rech *et al.*, 2006) (Figure 3A). Only those regions traversed by rivers originating in the high volcanic arc have deeply incised canyons (Zeilinger *et al.*, 2005; Hoke *et al.*, 2007; Schildgen *et al.*, 2007). In contrast, headwaters in the climatic transition zone between 28°S to 35°S are highly dissected. These sub-catchments have steep hillslopes, sharp ridges, and record a glacial overprint (Figure 3B). The catchments in the humid south between 35°S and 40°S display a smooth local relief with moderate hillslopes and subrounded ridges (Figure 3C). In contrast, south of 40°S the landscape has steeper hillslopes and a higher degree of dissection (Figure 3D). These observations are clearly reflected in our morphometric data, suggesting a strong influence of rainfall and snowline elevation on topography along the western flank of the Andean margin (Figures 4 and 5, Tables AI, AII and AIII in the Appendix).

Table I. Definition and sources of the calculated variables

Variable	Unit	Definition	Source
Vertical shape			
Profile concavity		Normalized area under the normalized distance-elevation profile (diagonal from source to mouth would be 0·5) PCI > 0·5 reflect a strongly convex profile	after Demoulin, 1998
Hypsometric integral		Normalized area under a normalized area-elevation curve after Strahler	after Strahler, 1952
Geometry			
Basin area	km^2	Area of the drainage basin	
Basin length	km	Longest distance from outlet	
Basin width	km	Longest distance perpendicular to basin length	
Basin form		Basin length/basin width	
Basin elongation ratio		Diameter of a circle with basin area/basin length	after Schumm, 1956
Relief			
Basin mean elevation	m	Average elevation calculated within a drainage basin	
Total basin relief	m	Basin maximum elevation – basin minimum elevation	
Basin relief ratio		relief/length × 100	
Basin local relief	m	Local relief averaged over a circle with a diameter of 10 cells	after Summerfield, 1991
Channel drop	m/m	(channel maximum elevation – channel minimum elevation)/channel length	
Climate			
Mean annual rainfall	mm/a		TRMM 30 km dataset
Mean annual temperature	°C		cru-dateset, 10′ grid (http://www.cru.uea.ac.uk/cru/date)
Mean annual ground frost	d/a		cru-dateset, 10′ grid (http://www.cru.uea.ac.uk/cru/date)
Modern perennial snowline	m		after Schwerdtfeger, 1976; Rabassa and Clapperton, 1990
Lowest Pleistocene glacier extern	m		after Schwerdtfeger, 1976; Rabassa and Clapperton, 1990
Erosion			
Erosion index		$e = Q^{0.5} \times S$, with Q = mean annual rainfall, S = channel drop	after Finlayson *et al.*, 2002
Erosion intensity	km^3/a	IE × A × S, with P = mean annual rainfall, A = drainage area	after Montgomery *et al.*, 2001

Note: We mainly concentrate on basin mean elevation, basin total and local relief, mean annual rainfall, and snowline as well as glacier extent.

In the following sections we (1) introduce the influence of rainfall on the topography of drainage basins, (2) address the impact of glaciations on basin topography, and (3) describe the effect of climate on basin morphometry.

The influence of rainfall on basin topography

South of 35°S local relief, total catchment relief, and basin mean elevations significantly decrease by 26 to 70% (Figure 5). This decrease correlates with a considerable increase of rainfall in this region. Generally, a decrease of elevations towards the south could also be related to the descending snowline and a glacial 'buzz-saw effect' (Brozovic *et al.*, 1997). However, most parts of the mountain belt in this region are presently not glaciated and the decrease of local relief starts in all catchments when rainfall amounts exceed ~800 mm/a (Figure 5). Moreover, the relationships between rainfall and relief parameters can also be observed in forearc and mountain-front basins that have not been influenced by glacial erosion during the Quaternary. Hence, the decrease in elevation appears in fact to be related to increasing rainfall. Essentially, local relief shows very low values where rainfall amounts are highest. These observations indicate that 800 mm/a of rainfall might be a critical threshold-rainfall amount for these lithologies above which the fluvial system is coupled to the hillslopes and efficiently erodes these environments. We therefore suggest that the low mountain-range relief in the zone between 35°S to 40°S is caused by efficient, protracted fluvial erosion characterized by prolonged channel incision and the coupling of channels and hillslopes.

The glacial imprint on basin topography

Our data shows negative correlations between snowline and Pleistocene glacier extent versus basin mean elevation and total relief (Figures 4G and 4H, Tables AI and AII in the Appendix). Between ~18°S and 28°S the modern snowline and the lowest extent of Pleistocene glaciation lie well above the maximum elevations of the ranges (Figure 5). In contrast, basins south of ~27°S (arc catchments), ~28°S (sub-catchments), and ~32°S (mountain-front catchments) have been at least partially glaciated during the Pleistocene (Figure 5). Most

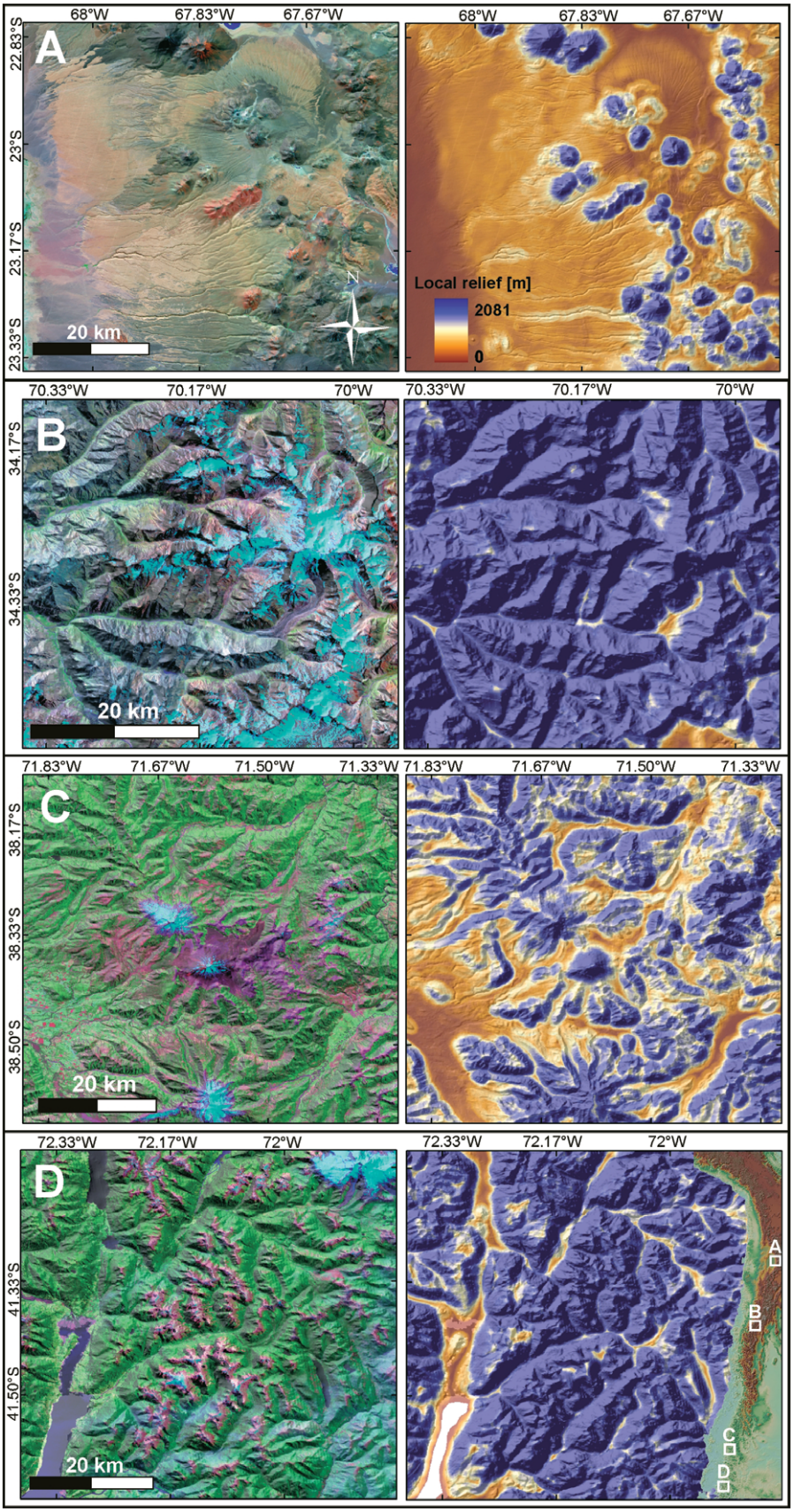

Figure 3. Landsat TM images in the left column and corresponding local relief map in the right column showing one typical headwater basins of each climatic zone. The inset in the lower right corner delineates the location of the close-ups. (A) Hyper-arid subtropical desert belt. Note the absence of incision and the low local relief in this transport-limited setting. (B) Arid-semiarid transition zone. Note the highly dissected landscape, steep hillslopes, and sharp ridges forming a high local relief. (C) Humid, temperate climate. Note the moderate hillslopes, smooth ridges, sediment-filled valleys, and generally decreased dissection and local relief. (D) Humid, cold region. Note the increased local relief expressed in steeper valleys, dissected landscape, and pronounced ridges [The inset of locations is added to part D of Figure 3 after the initial online publication]. This figure is available in colour online at wileyonlinelibray.com

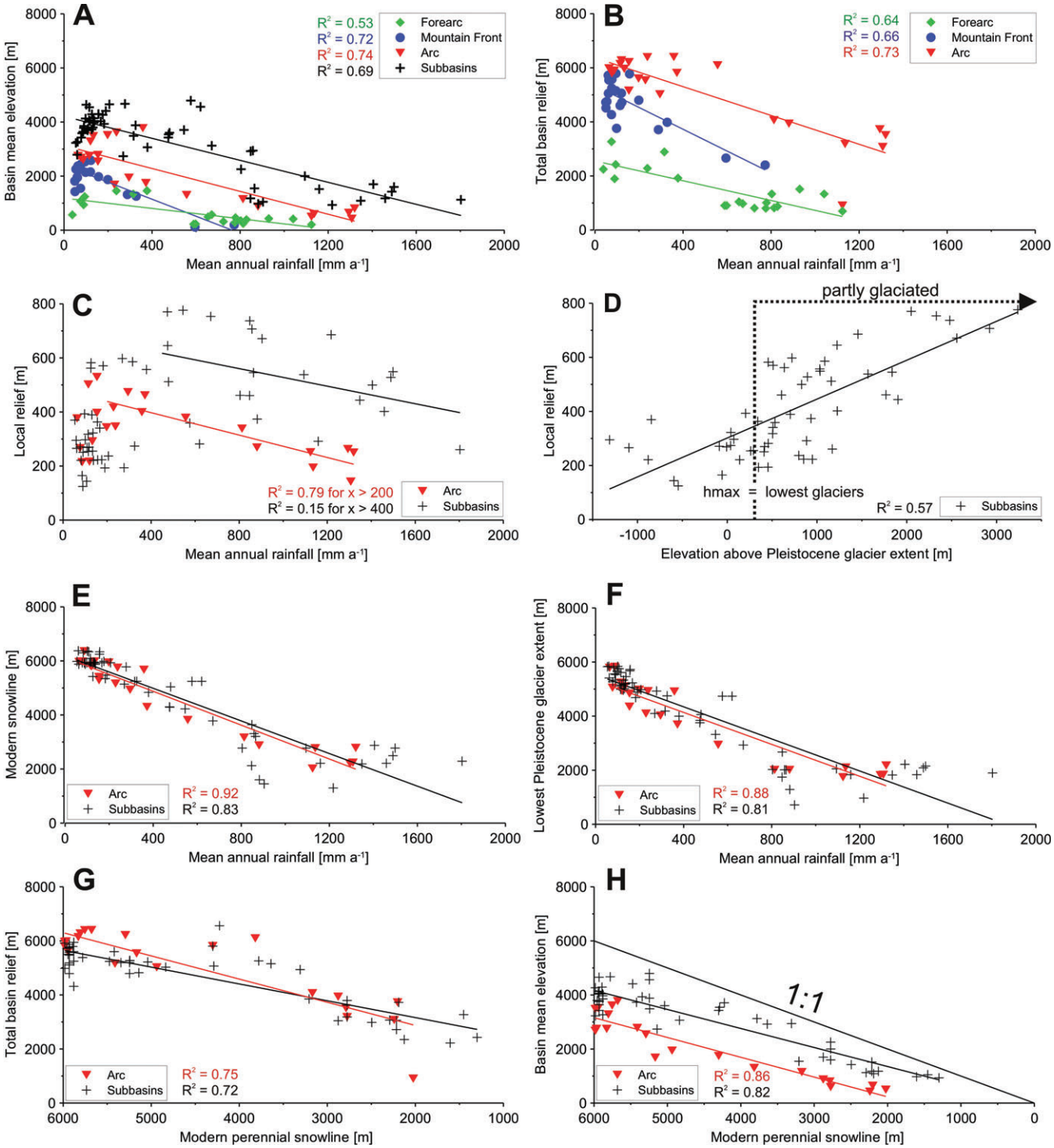

Figure 4. Correlations between relief and climate variables. The graphs (A) and (B) show a negative relationship between total basin relief as well as basin mean elevation versus rainfall. The graphs (A)–(C) and (E)–(H) are broadly north-south oriented from left to right. Note the inverse *x*-axes of the relief variables versus snowline (G, H). Graph (D) shows that the local relief increases the higher the basins reach above the Pleistocene glacier extent. Note the close relationship between snowline and glaciers versus rainfall (E, F). The correlation between HI and PCI versus rainfall is probably partly determined by relief parameters. HI, for example, is coupled to basin mean elevation, which itself is correlated with rainfall. This figure is available in colour online at wileyonlinelibrary.com

interestingly, in the region between 28°S and 35°S, where mean annual rainfall amounts are low, local relief displays a prominent maximum (Figure 5). In fact, once the maximum elevation is undercut by the snowline, basin sectors above this line display a progressive increase in local relief, hence the topography above the snowline gets progressively steeper (Figure 4D). We therefore suggest that the high local relief between 28°S and 35°S is the result of repeated glacial erosion during Quaternary times. The steep topography and high local relief can also be observed in catchment parts that are recently not glaciated (Figures 3 and 5). Interestingly, this implies that between 28°S and 35°S the present relief shows a clear imprint of past climatic episodes. The preservation might have been promoted by the present-day low rainfall amounts and inefficient erosion.

Both, modern and Pleistocene ELA start to descend southward when rainfall amounts increase along the western Andean flank (Figures 4E and 4F), which is dominated by

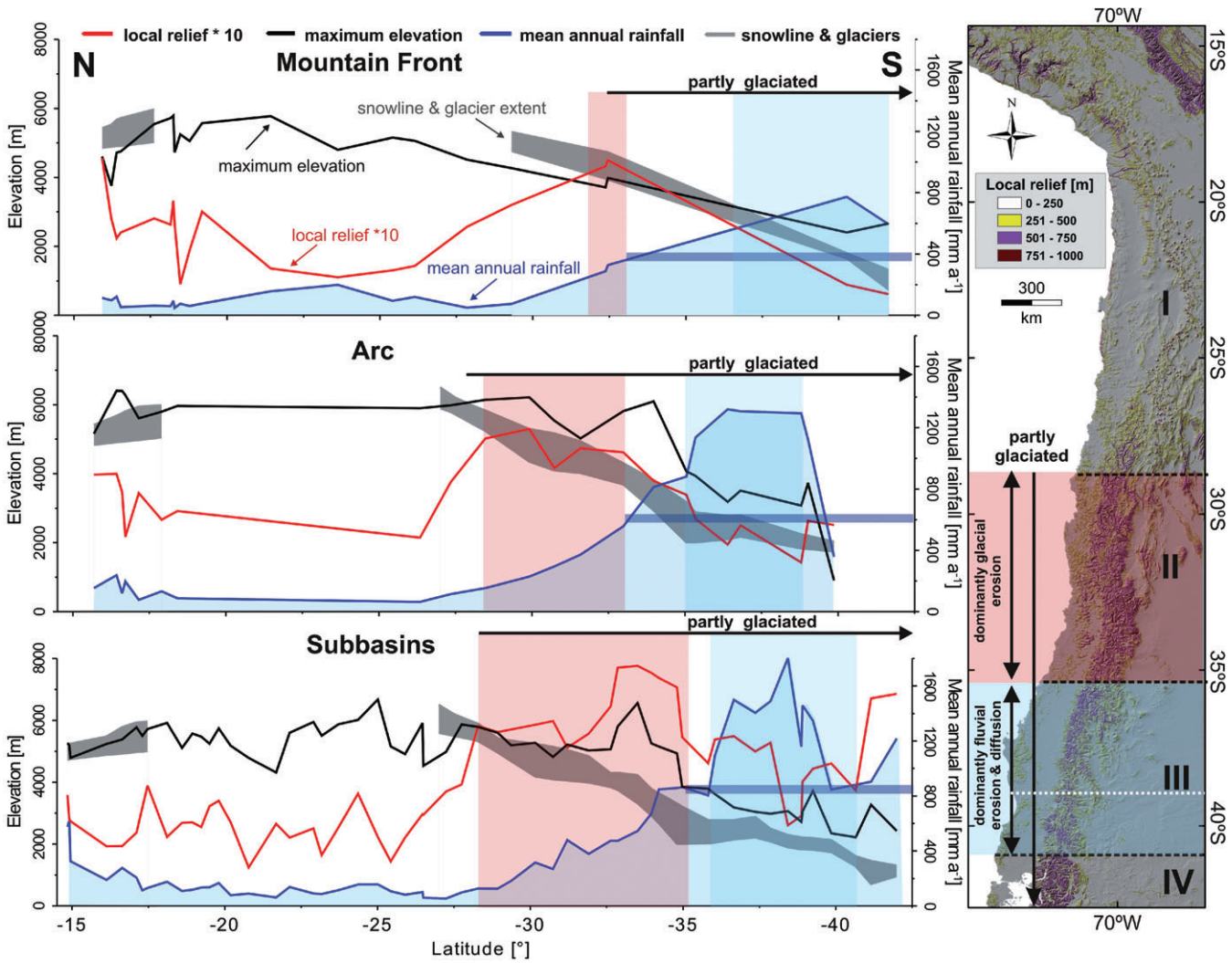

Figure 5. North-south distribution of relief and climate parameters. Note the local-relief maximum around 28°S to 35°S coinciding with increasing rainfall in the arid-semiarid transition zone and the undercutting of the basin maximum elevations by the snowline and the lowest Pleistocene glacier extent (red rectangle). When rainfall amounts increase and exceed ~800 mm/a (blue bar) local relief is reduced and maximum elevations drop significantly. Local relief reaches a minimum around 35°S to 40°S where rainfall rates are highest. This suggests a glacially dominated high-relief landscape where rainfall is low (~28°S–35°S) and a fluvially dominated low-relief landscape where erosion is efficient due to high rainfall amounts (~35°S–40°S). South of 40°S local relief appears to rise again in the sub-catchments. The right map shows the local relief sectors in roman numbers. Note the enhanced local relief in sector II (Figure 4B) and the smoothed relief in sector III (Figure 4C). The thin dotted lines indicate tectonic segments. South of ~27°S catchments are partially influenced by glaciation. The region between 28°S to 35°S is dominated by glacial erosion, the region between 35°S and 40°S by fluvial erosion and diffusive denudation. This figure is available in colour online at wileyonlinelibrary.com

westerly sourced moisture south of 28°S (Clapperton, 1994; Haselton *et al.*, 2002). Thus, northward-migrating Westerlies may have reached these latitudes, intensifying precipitation during glacial periods and delivering sufficient moisture for glaciation in these threshold environments (e.g. Heusser, 1989; Lamy *et al.*, 1999). This supports the notion that glaciation in large parts of the Central Andes is moisture-controlled, which is in good agreement with results from Haselton *et al.* (2002) who concluded that the Pleistocene snowline in the southern Altiplano-Puna Plateau is more sensitive to moisture increase than temperature.

Relations between climate and basin morphometry

Variables describing the geometric shape of drainage basins do not show correlations with climatic parameters (Table AI in the Appendix). In contrast, the vertical shape of basins appears to be strongly affected by climate. PCI and HI are reduced with enhanced rainfall (Table AIII in the Appendix). The inverse relationships between rainfall and PCI as well as rainfall and HI probably reflect more efficient erosion at higher rainfall rates, where rivers and hillslopes adjust faster to changes in boundary conditions and approach equilibrium. Our data thus supports studies, suggesting that sparse precipitation correlates with convex profiles (high PCI), whereas concave profiles (low PCI) develop in regions with intense rainfall (Roe *et al.*, 2002; Zaprowski *et al.*, 2005). HI scales with mean elevation and rainfall (Table AIII in the Appendix). This corroborates the idea that the HI actually reflects the efficiency of erosion processes, not necessarily the age of landscapes. Hence, in synoptic studies of mountain belts in similar climatic settings HI-values should rather be used relative to each other as proxies for tectonic activity as indicated by results of Montgomery *et al.* (2001).

Table II. Relief reduction due to a doubling of rainfall

Mean annual rainfall (mm/a)	△ Mean elevation (%)	△ Total relief (%)	Position
50–100	118	8	Forearc
	18	–20	Mountain front
	0	3	Arc
	44	–37	Subbasins
	45	–12	Average
100–200	–24	–38	Forearc
	–13	28	Mountain front
	28	–9	Arc
	0	7	Subbasins
	–2	–3	Average
200–400	55	29	Forearc
	–33	–17	Mountain front
	–50	4	Arc
	–34	91	Subbasins
	–16	27	Average
400–800	–76	–31	Forearc
	–85	–40	Mountain front
	–34	–30	Arc
	–26	–27	Subbasins
	–55	–32	Average
800–1600	<–41	<–48	Forearc
	—	—	Mountain front
	<–30	<–14	Arc
	–29	–10	Subbasins
	–33	–24	Average
>400	–44	–28	Average

Note: See the amount of rainfall and the respective change in mean elevation and total relief for each basin group. Note that mean elevation and total relief are only significantly reduced by doubling rainfall amounts above rainfall rates of 400 mm/a.

Discussion

Our results are in agreement with other empirical and modeling studies, which propose that high precipitation rates lower elevation and relief (e.g., Montgomery *et al.*, 2001; Roe *et al.*, 2003; Gabet *et al.*, 2004). Roe *et al.* (2003) suggest that in rainfall-dominated environments a mountain range can be lowered by more than half due to enhanced precipitation. In the tectonically active Himalaya, Gabet *et al.* (2004) document that a doubling of annual rainfall from 2000 to 4000 mm results in a 33% decrease in total relief. Despite significantly lower rainfall amounts in the study area on the western Andean flank, our results document a decrease in mean elevation and total relief on the order of 44% and 28%, respectively, for a doubling of rainfall amounts (Table II). Such a rainfall-induced decrease in elevation and enhanced erosivity might be controlled by an increase in drainage density (e.g. Tucker and Bras, 1998; Whipple *et al.*, 1999). In fact, in the study area enhanced rainfall is associated with a progressive southward increase of drainage density (Figure 6). High drainage density causes more effective denudation of higher catchment parts that are not integrated in the fluvial network when drainage density is low (Figure 6). As a result, in fluvially dominated areas total and local relief decrease with increasing drainage density and increasing rainfall.

Consequently, we distinguish two geomorphic sectors on the western flank of the Central to Southern Andes. Between 35°S and 40°S fluvial erosion, enhanced by high protracted rainfall amounts, appears to be very efficient. As a result, local relief is diminished (Figure 5). In contrast, between 28°S to 35°S rainfall amounts are below a critical threshold, rendering fluvial erosion ineffective. Based on our data we conclude that the pronounced high local relief has been generated by glacial erosion during the Quaternary. This implies that the topography we observe today is a relict from past climatic episodes. Hence, the region between 28°S and 35°S appears to be a transient landscape, which does not reflect the presently prevailing geomorphic processes.

Clearly, erosion and topography in active mountain belts are also determined by tectonic processes. Due to the lack of uplift data in the Main Cordillera, we applied the shortening rate as a proxy for potential surface deformation. This complicates the comparison of tectonic processes. However, changes in shortening rate imply basic changes in deformation processes and can thus be regarded as tectonic boundary conditions. In principle, the Andean shortening rate decreases southward, absolute shortening is reduced by more than 30% from high shortening (>300 km) to low shortening (<100 km) at around 30°S (e.g. Allmendinger *et al.*, 1990; Vietor and Echtler, 2006) (Figure 1). We observe the local relief maximum at 28°S to 35°S, and thereby already in a sector where shortening is low. This is the opposite of what might be expected if shortening would be the controlling factor for enhanced local relief. In addition, the flat-slab segment does not coincide with the low-relief topography between 28°S and 35°S. Consequently, the sectors defined by high local relief and dominant geomorphic process are not consistent with tectonic segments. Finally, the high-relief sector does not correlate with a distinct rock type characterized by low erodibility, but mainly comprises Cretaceous to Miocene volcano-sedimentary and volcanic rocks, which are abundant in large parts of the Andes (Servicio Nacional de Geológía y Minería, 2003). A lithologic control on general morphologic and topographic trends can thus be excluded as well. In summary, neither changes in shortening rate, subduction properties, and lithology

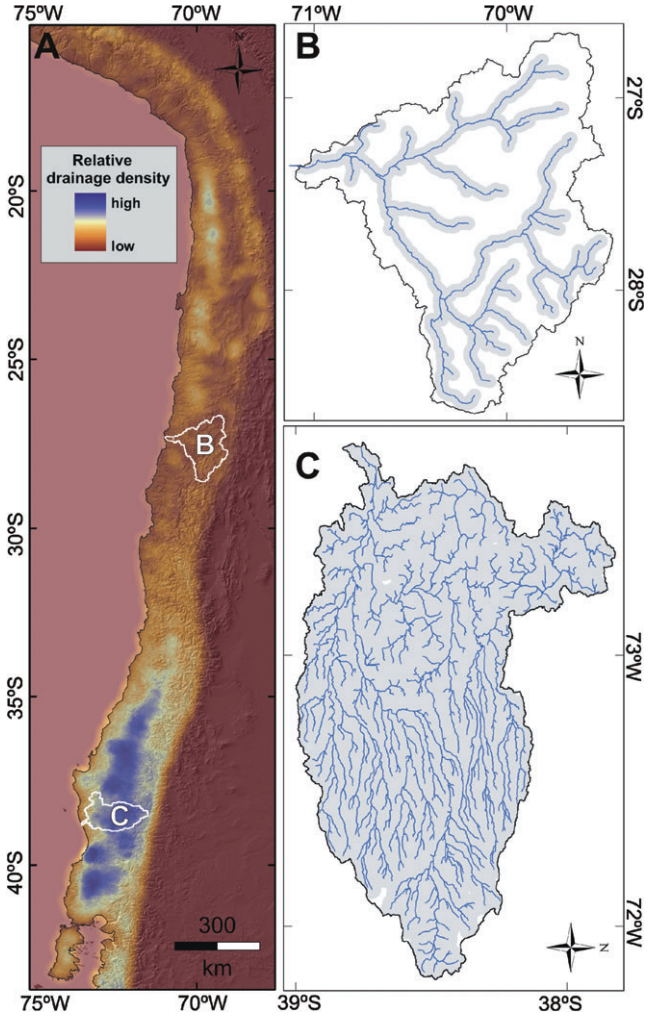

Figure 6. (A) Relative drainage density along the margin calculated as the cumulative channel length per unit area. On the right see close-ups of two catchments representative for the arid (B) and humid (C) part of the study area. Note the significantly higher drainage density in the south where rainfall amounts are increased. The grey-shaded regions in basins (B) and (C) outline the parts of the catchments that are integrated in the fluvial network and thus denudated. In catchments with a higher drainage density in the south the entire basin with all hillslopes is integrated whereas dry catchments in the north display distinct ridges and interfluves not reached by the drainage network. This figure is available in colour online at wileyonlinelibrary.com

nor the spatial distribution of deformation can solely account for the high local relief sector. This suggests that local relief along the Andean margin is mainly the result of surface processes determined by present and past climatic conditions. Especially the zone between 28°S and 35°S appears to show a prominent imprint of transient climate episodes.

Conclusion

We analyzed climatic and topographic parameters of 120 drainage basins along the western Andean flank between 15·5°S and 41·5°S based on SRTMV3-90m topographic data and the new medium spatial resolution satellite-derived TRMM dataset. In order to diagnose the imprint of different climatic zones on the relief of mountain ranges, we correlated climatic with relief parameters and investigated the impact of different geomorphic regimes on relief evolution.

Our results suggest that (1) increased rainfall diminishes mean and maximum elevations of mountain ranges and provide a compelling support for the idea that drainage density is a key parameter in landscape evolution. In fact, the observed decrease of elevations appears to be caused by the high drainage density in humid regions, which enables the integration of the entire catchment in the fluvial network and thereby the efficient coupling of channels and hillslopes. Additionally, our data indicates that (1) glacial erosion increases basin relief and limits total range topography. This might be caused by focusing erosion on summits and ridges above the ELA. Eventually, our analyses show that (2) PCI and the HI strongly depend on rainfall, while the geometric basin shape appears not to be affected by climate.

Consequently, our study suggests that the generation of local relief is a force balance between protracted fluvial erosion and glacial erosion. In this respect, the two processes act as opposite agents. Whereas glacial erosion appears to create local relief, persistent moderate rainfall above a critical threshold appears to smooth it.

Overall, we conclude that the catchment-scale relief of the western flank of the Andean mountain chain distinctly reflects the dominant geomorphic process, which is determined by and therefore represents past and present regional climatic regimes. Notwithstanding, we do not challenge that the large-scale architecture of the Andes is maintained by tectonic processes and the reactivation of inherited basement structures. The geomorphic signature of the Western Andes between 28°S and 35°S, however, expresses significant transient components, which may reflect erosion processes under different climatic conditions during the geologic past. In general, basin topography could thus be used to identify the efficiency of past paleoclimatic conditions and geomorphic processes.

Acknowledgements—This work was funded by Deutsche Forschungsgemeinschaft through the Leibniz Award to M.R. Strecker (STR373-16-1), the A. Cox fund of Stanford University, and the GeoForschungsZentrum Potsdam as well as the DAAD, the German Academic Exchange Program, to K. Rehak. We appreciate discussions with G. Hilley.

References

Allmendinger RW, Figueroa O, Snyder D, Beer J, Mpodozis C, Isacks BL. 1990. Foreland shortening and crustal balancing in the Andes at 30°S latitude. *Tectonics* **9**(4): 789–809.

Allmendinger RW, Jordan TE, Kay SM, Isacks BL. 1997. The evolution of the Altiplano-Puna plateau of the Central Andes. *Annual Review of Earth and Planetary Sciences* **25**: 139–174.

Ammann C, Jenny B, Kammer K, Messerli B. 2001. Late Quaternary Glacier response to humidity changes in the arid Andes of Chile (18–29 degrees S). *Palaeogeography Palaeoclimatology Palaeoecology* **172**(3–4): 313–326.

Angermann D, Klotz J, Reigber C. 1999. Space-geodetic estimation of the Nazca-South America Euler vector. *Earth and Planetary Science Letters* **171**(3): 329–334.

Atwater BF, Jiménez Núnez H, Vita-Finzi C. 1992. Net late Holocene emergence despite earthquake-induced submergence, south-central Chile. *Quaternary International* **15/16**: 77–85.

Bangs NL, Cande SC. 1997. Episodic development of a convergent margin inferred from structures and processes along the southern Chile margin. *Tectonics* **16**(3): 489–503.

Bice KL, Scotese CR, Seidov D, Barron EJ. 2000. Quantifying the role of geographic change in Cenozoic ocean heat transport using uncoupled atmosphere and ocean models. *Palaeogeography Palaeoclimatology Palaeoecology* **161**: 295–310.

Blisniuk PM, Stern LA, Chamberlain CP, Idleman B, Zeitler PK. 2005. Climatic and ecologic changes during Miocene surface uplift in the Southern Patagonian Andes. *Earth and Planetary Science Letters* **230**(1–2): 125–142.

Bookhagen B, Echtler HP, Melnick D, Strecker M, Spencer JQG. 2006. Using uplifted Holocene beach berms for paleoseismic analysis on the Santa Maria Island, south-central Chile. *Geophysical Research Letters* **33**(15). DOI. 10.1029/2006GL026734.

Bookhagen B, Strecker M. 2008. Orographic barriers, high-resolution TRMM rainfall, and relief variations along the eastern Andes. *Geophysical Research Letters* **35**. DOI. 10.1029/2007GL032011.

Brooks BA, Bevis M, Smalley RJ, Kendrick E, Manceda R, Lauria E, Manturana R, Araujo M. 2003. Crustal motion in the Southern Andes (26°–36°S): do the Andes behave like a microplate? *Geochemical Geophysical Geosystems* **4**(10). DOI. 10.1029.

Brozovic N, Burbank DW, Meigs AJ. 1997. Climatic limits on landscape development in the northwestern Himalaya. *Science* **276**(5312): 571–574.

Büdel J. 1982. *Climatic Geomorphology*. Princeton University Press: Princeton, NJ; 443 pp.

Cembrano J, Schermer E, Lavenu A, Sanhueza A. 2000. Contrasting nature of deformation along an intra-arc shear zone, the Liquine-Ofqui fault zone, southern Chilean Andes. *Tectonophysics* **319**(2): 129–149.

Champagnac JD, Molnar P, Anderson RS, Sue C, Delacou B. 2007. Quaternary erosion-induced isostatic rebound in the western Alps. *Geology* **35**(3): 195–198.

Charrier R, Pinto L, Rodriguez MP. 2007. Tectonostratigraphic evolution of the Andean Orogen in Chile. In *The Geology of Chile*, Moreno T, Gibbons W (eds). The Geological Society: London; 440 pp.

Clapperton CM. 1993. Nature of environmental changes in South America at the last glacial maximum. *Palaeogeography Palaeoclimatology Palaeoecology* **101**(3–4): 189–208.

Clapperton CM. 1994. The Quaternary glaciation of Chile – a review. *Revista Chilena de Historia Natural* **67**(4): 369–383.

Demets C, Gordon RG, Argus DF, Stein S. 1994. Effect of recent revisions to the geomagnetic reversal timescale on estimates of current plate motions. *Geophysical Research Letters* **21**(20): 2191–2194.

Demoulin A. 1998. Testing the tectonic significance of some parameters of longitudinal river profiles: the case of the Ardenne (Belgium, NW Europe). *Geomorphology* **24**(2–3): 189–208.

Dewey JF, Lamb SH. 1992. Active tectonics of the Andes. *Tectonophysics* **205**: 79–95.

Diraison M, Cobbold PR, Rossello EA, Amos AJ. 1998. Neogene dextral transpression due to oblique convergence across the Andes of northwestern Patagonia, Argentina. *Journal of American Earth Sciences* **11**(6): 519–532.

Dunai TJ, Lopez GAG, Juez-Larre J. 2005. Oligocene-Miocene age of aridity in the Atacama Desert revealed by exposure dating of erosion-sensitive landforms. *Geology* **33**(4): 321–324.

Farias M, Charrier R, Comte D, Martinod J, Herail G. 2005. Late Cenozoic deformation and uplift of the western flank of the Altiplano: evidence from the depositional, tectonic, and geomorphologic evolution and shallow seismic activity (northern Chile at 19 degrees 30′ S). *Tectonics* **24**(4). DOI. 10.1029/2006TC002046.

Finlayson DP, Montgomery DR, Hallet B. 2002. Spatial coincidence of rapid inferred erosion with young metamorphic massifs in the Himalayas. *Geology* **30**(3): 219–222. DOI. 10.1130/0091-7613(2002)030

Gabet EJ, Pratt-Sitaula BA, Burbank DW. 2004. Climatic controls on hillslope angle and relief in the Himalayas. *Geology* **32**(7): 629–632.

Garreaud R, Vuille M, Clement AC. 2003. The climate of the Altiplano: observed current conditions and mechanisms of past changes. *Palaeogeography Palaeoclimatology Palaeoecology* **194**(1–3): 5–22.

Glodny J, Lohrmann J, Echtler H, Gräfe K, Seifert W, Collao S, Figueroa O, 2005. Internal dynamics of an accretionary wedge: insights from combined isotope tectonochronology and sandbox modelling of the South-Central Chilean forearc. *Earth and Planetary Science Letters* **231**(1–2): 23–39.

Glodny J, Gräfe K, Echtler H, Rosenau M. 2008. Mesozoic to Quaternary continental margin dynamics in South-Central Chile (36°–42°S): the apatite and zircon fission track perspective. *International Journal of Earth Sciences* **97**(6): 1271–1291. DOI 10.1007/s00531-007-0203-1.

Hallet B, Hunter L, Bogen J. 1996. Rates of erosion and sediment evacuation by glaciers: a review of field data and their implications. *Global and Planetary Change* **12**(1–4): 213–235.

Hartley AJ. 2003. Andean uplift and climate change. *Journal of the Geological Society* **160**: 7–10.

Hartley AJ, Chong G. 2002. Late Pliocene age for the Atacama Desert: implications for the desertification of western South America. *Geology* **30**(1): 43–46.

Haselton K, Hilley G, Strecker MR. 2002. Average Pleistocene climatic patterns in the southern central Andes: controls on mountain glaciation and paleoclimate implications. *Journal of Geology* **110**(2): 211–226.

Hebbeln D, Lamy F, Mohtadi M, Echtler H. 2007. Tracing the impact of glacial-interglacial climate variability on erosion of the southern Andes. *Geology* **35**(2): 131–134.

Hervé AF. 1988. Late Paleozoic subduction and accretion in southern Chile. *Episodes* **11**(3): 183–188.

Hervé AF, Faundex V, Calderón M, Massonne HJ, Willner AP. 2007. Metamorphic and plutonic basement complexes. In *The Geology of Chile*, Moreno T, Gibbons W (eds). The Geological Society: London; 440 pp.

Heusser CJ. 1989. Southern Westerlies during the last glacial maximum. *Quaternary Research* **31**(3): 423–425.

Hoke GD, Isacks BL, Jordan TE, Blanco N, Tomlinson AJ, Ramezani J. 2007. Geomorphic evidence for post-10 Ma uplift of the western flank of the central Andes 18 degrees 30′–22 degrees S. *Tectonics* **26**: 192–201.

Huffman GJ, Adler RF, Bolvin DT, Gu G, Nelkin EJ, Bowman KP, Hong Y, Stocker EF, Wolff DB. 2007. The TRMM Multi-satellite Precipitation Analysis: Quasi-global, multi-year, combined-sensor precipitation estimates at fine scale. *J. Hydrometeor.*, **8**(1): 38–55.

Isacks B. 1988. Uplift of the Central Andean Plateau and bending of the Bolivian Orocline. *Journal of Geophysical Research* **93**(B4): 3211–3231.

Jenny B, Valero-Garces BL, Villa-Martinez R, Urrutia R, Geyh M, Veit H. 2002. Early to mid-Holocene aridity in central Chile and the southern Westerlies: the Laguna Aculeo record (34 degrees S). *Quaternary Research* **58**(2): 160–170.

Jordan TE. 1993. Chronology of motion in a complete thrust belt: the Precordillera, 30–31°S, Andes Mountains. *Journal of Geology* **101**(2): 135–156.

Jordan TE, Bryan LI, Allmendinger RW, Brewer JA, Ramos VA, Ando CJ. 1983. Andean tectonics related to geometry of subducted Nazca plate. *Geological Society of America Bulletin* **94**: 341–361.

Jordan TE, Allmendinger RW. 1986. The Sierras Pampeanas of Argentina – a modern analog of Rocky-Mountain foreland deformation. *American Journal of Science* **286**(10): 737–764.

Kaizuka S, Matsuda T, Nogami M, Yonekura N. 1973. *Quaternary Tectonic and Recent Seismic Crustal Movements in the Arauco Peninsula and its Environs, Central Chile*, Geographical Report 8. Tokyo Metropolitan University: Tokyo; 1–49.

Kay SM, Mpodozis C. 2002. Magmatism as a probe to the Neogene shallowing of the Nazca plate beneath the modern Chilean flat-slab. *Journal of South American Earth Sciences* **15**(1): 39–57.

Kirby E, Whipple K. 2001. Quantifying differential rock-uplift rates via stream profile analysis. *Geology* **29**(5): 415–418.

Kley J, Monaldi CR. 1998. Tectonic shortening and crustal thickness in the Central Andes: how good is the correlation? *Geology* **26**(8): 723–726.

Kley J, Monaldi CR, Salfity JA. 1999. Along-strike segmentation of the Andean foreland: causes and consequences. *Tectonophysics* **301**(1–2): 75–94.

Klotz J, Khazaradze G, Angermann D, Reigber C, Perdomo R, Cifuentes O. 2001. Earthquake cycle dominates contemporary crustal deformation in central and southern Andes. *Earth and Planetary Science* Letters **193**(3–4): 437–446.

Kummerow C, Simpson J, Thiele O, Barnes W, Chang ATC, Stocker E, Adler RF, Hou A, Kakar R, Wentz F, Ashcroft P, Kozu T, Hong Y, Okamoto K, Iguchi T, Kuroiwa H, Im E, Haddad Z, Huffman G, Ferrier B, Olson WS, Zipser E, Smith EA, Wilheit TT, North G, Krishnamurti T, Nakamura K. 2000. The status of the Tropical Rainfall Measuring Mission (TRMM) after two years in orbit. *Journal of Applied Meteorology* **39**: 1965–1982.

Lamy F, Hebbeln D, Wefer G. 1998. Late quaternary precessional cycles of terrigenous sediment input off the Norte Chico, Chile (27.5

degrees S) and palaeoclimatic implications. *Palaeogeography Palaeoclimatology Palaeoecology* **141**(3–4): 233–251.

Lamy F, Hebbeln D, Wefer G. 1999. High-resolution marine record of climatic change in mid-latitude Chile during the last 28,000 years based on terrigenous sediment parameters. *Quaternary Research* **51**(1): 83–93.

Lamy F, Klump J, Hebbeln D, Wefer G. 2000. Late Quaternary rapid climate change in northern Chile. *Terra Nova* **12**(1): 8–13.

Le Roux JP, Gómez C, Venegas C, Fenner J, Middleton H, Marchant M, Buchbinder B, Frassinetti D, Marquardt C, Gregory-Wodzicki KM, Lavenu A. 2005. Neogene-Quaternary coastal and offshore sedimentation in north central Chile: record of sea-level changes and implications for Andean tectonism. *Journal of South American Earth Sciences* **19**: 83–89.

Le Roux JP, Olivares DM, Nielsen SN, Smith ND, Middleton H, Fenner J, Ishman SE. 2006. Bay sedimentation as controlled by regional crustal behaviour, local tectonics, and eustatic sea-level changes: Coquimbo Formation (Miocene-Pliocene), Bay of Tongoy, central Chile. *Sedimentary Geology* **184**: 133–153.

Marquardt C, Lavenu A, Ortlieb L, Godoy E, Comte D. 2004. Coastal neotectonics in southern central Andes: uplift and deformation of marine terraces in northern Chile (27 degrees S). *Tectonophysics* **394**(3–4): 193–219.

Melnick D, Bookhagen B, Echtler H, Strecker M. 2006. Coastal deformation and great subduction earthquakes, Isla Santa María, Chile (37°S). *Geological Society of America Bulletin* **118**(11): 1463–1480.

Melnick D, Echtler H. 2006. Inversion of forearc basins in south-central Chile caused by rapid glacial age trench fill. *Geology* **34**(9): 709–712.

Melnick D, Bookhagen B, Strecker MR, Echtler HP. 2009. Segmentation of megathrust rupture zones from fore-arc deformation patterns over hundreds to millions of years, Arauco peninsula, Chile. *Journal of Geophysical Research* **114**(B1). DOI. 10.1029/2008JB005788.

Mitchell SG, Montgomery DR. 2006. Influence of a glacial buzzsaw on the height and morphology of the Cascade Range in central Washington State, USA. *Quaternary Research* **65**(1): 96–107.

Molnar P, England P. 1990. Late Cenozoic uplift of nountain ranges and global climate change – chicken or egg. *Nature* **346**(6279): 29–34.

Montgomery DR, Balco G, Willett SD. 2001. Climate, tectonics, and the morphology of the Andes. *Geology* **29**(7): 579–582.

Montgomery DR, Brandon MT. 2002. Topographic controls on erosion rates in tectonically active mountain ranges. *Earth and Planetary Science Letters* **201**(3–4): 481–489.

Mpodozis C, Ramos VA. 1989. The Andes of Chile and Argentina. In *Geology of the Andes and its Relation to Hydrocarbon and Mineral Resources*, Ericksen G, Canas Pinochet M, Reinemund J (eds). Earth Science Series – Circum-Pacific Council of Energy and Mineral Resources: Houston, TX; 59–89.

Muñoz J, Troncoso R, Duhart P, Crignola P, Farmer L, Stern CR. 2000. The relation of the mid-Tertiary coastal magmatic belt in south-central Chile to the late Oligocene increase in plate convergence rate. *Revista Geologica de Chile* **27**(2): 177–203.

Nelson AR, Manley WF. 1992. Holocene coseismic and aseismic uplift of Isla Mocha, south-central Chile. Impacts of tectonics on Quaternary coastal evolution. *Quaternary International* **15–16**: 61–76.

New M, Lister D, Hulme M, Makin I. 2002. A high-resolution data set of surface climate over global land areas. *Climate Research* **21**(1): 1–25.

Nishiizumi K, Caffee MW, Finkel RC, Brimhall G, Mote T. 2005. Remnants of a fossil alluvial fan landscape of Miocene age in the Atacama Desert of northern Chile using cosmogenic nuclide exposure age dating. *Earth and Planetary Science Letters* **237**(3–4): 499–507.

Ohmori H. 1993. Changes in the hypsometric curve through mountain building resulting from concurrent tectonics and denudation. *Geomorphology* **8**: 263–277.

Oncken O, Hindle D, Kley J, Elger K, Victor V, Schemmann K. 2006. Deformation of the Central Andean upper plate system – facts, fiction, and constraints for plateau models. In *The Andes – active subduction orogeny. Volume 1: Frontiers in Earth Science Series*, Oncken O, Chong G, Frank G, Giese P, Götze HJ, Ramos VA, Strecker MR, Wigger P (eds). Springer-Verlag: Berlin; 287 pp.

Ortlieb L, Diaz A, Guzman N. 1996a. A warm interglacial episode during oxygen isotope stage 11 in northern Chile. *Quaternary Science Reviews* **15**: 857–871.

Ortlieb L, Zazo C, Goy JL, HillaireMarcel C, Ghaleb B, Cournoyer L. 1996b. Coastal deformation and sea-level changes in the northern Chile subduction area (23 degrees S) during the last 330 ky. *Quaternary Science Reviews* **15**(8–9): 819–831.

Pankhurst RJ, Hervé F. 2007. Introduction and overview. In *The Geology of Chile*, Moreno T. Gibbons W. (eds). The Geological Society: London; 440 pp.

Parada MA. 1990. Granitoid plutonism in central Chile and its geodynamic implications: a review. In *Plutonism from Antarctica to Alaska, volume 241*. Geological Society of America: Boulder, CO; 51–66.

Pino M, Navarro RX. 2005. Geoarquelogía del sitio arcaico Chan-Chan 18, costa de Valdivia: Discriminación de ambientes de ocupación humana y su relación con la transgresión marina del Holoceno Medio. *Revista Geologica de Chile* **32**: 59–75.

Purves RS, Korup O. 2007. Multiscale analysis of hillslope height for geomorphometry. In Proceedings of GISRUK 2007, Winstanley AC. (eds). Maynooth: Ireland; 484–488.

Rabassa J, Clapperton CM. 1990. Quaternary glaciations of the southern Andes. *Quaternary Science Reviews* **9**(2–3): 153–174.

Radtke U. 1989. *Marine Terrassen und Korallenriffe – Das Problem der quartären Meeresspiegelschwankungen erläutern an Fallstudien aus Chile, Argentinien und Barbados*. Heinrich-Heine-Universität: Dusseldorf.

Ramos VA, Cristallini EO, Perez DJ. 2002. The Pampean flat-slab of the Central Andes. *Journal of South American Earth Sciences* **15**(1): 59–78.

Rech JA, Currie BS, Michalski G, Cowan AM. 2006. Neogene climate change and uplift in the Atacama Desert, Chile. *Geology* **34**(9): 761–764.

Rehak K, Strecker M, Echtler H. 2008. Morphotectonic segmentation of an active forearc, 37°–41°S, Chile. *Geomorphology* **94**: 98–116.

Rehak K, Niedermann S, Preusser F, Strecker MR, Echtler HP. In press. Late Pleistocene landscape evolution in south-central Chile constrained by luminescence and stable cosmogenic nuclide dating. *GSA Bulletin*.

Reiners PW, Ehlers TA, Mitchell SG, Montgomery DR. 2003. Coupled spatial variations in precipitation and long-term erosion rates across the Washington Cascades. *Nature* **426**(6967): 645–647.

Roe GH, Montgomery DR, Hallet B. 2002. Effects of orographic precipitation variations on the concavity of steady-state river profiles. *Geology* **30**(2): 143–146.

Roe GH, Montgomery DR, Hallet B. 2003. Orographic precipitation and the relief of mountain ranges. *Journal of Geophysical Research-Solid Earth* **108**(B6). DOI. 10.1029/2001JB001521

Romero OE, Kim JH, Hebbeln D. 2006. Paleoproductivity evolution off central Chile from the Last Glacial Maximum to the Early Holocene. *Quaternary Research* **65**: 519–525.

Rosenau M, Melnick D, Echtler H. 2006. Kinematic constraints on intra-arc shear and strain partitioning in the Southern Andes between 38 degrees S and 42 degrees S latitude. *Tectonics* **25**(4): TC4013.

Schildgen TF, Hodges KV, Whipple KX, Reiners PW, Pringle MS. 2007. Uplift of the western margin of the Andean plateau revealed from canyon incision history, southern Peru. *Geology* **35**(6): 523–526.

Scholl DW, Christen M, von Huene R, Marlow MS. 1970. Peru-Chile trench sediments and sea-floor spreading. *Geological Society of America Bulletin* **81**(5): 1339ff.

Schumm SA. 1956. Evolution of drainage systems and slopes in badlands at Perth Amboy, New Jersey. *Bulletin of the Geological Society of America* **67**: 597–646.

Schwerdtfeger W. 1976. *Climates of Central and South America*. Elsevier: Amsterdam.

Servicio Nacional de Geológía y Minería. 2003. *Mapa geológico de Chile*. Talleres Gráficos Instituto Geográfico Militar: Santiago.

Small EE, Anderson RS. 1998. Pleistocene relief production in Laramide mountain ranges, western United States. *Geology* **26**(12): 1151–1152.

Snyder NP, Whipple KX, Tucker GE, Merritts DJ. 2000. Landscape response to tectonic forcing: digital elevation model analysis of stream profiles in the Mendocino triple junction region, northern California. *Geological Society of America Bulletin* **112**(8): 1250–1263.

Somoza R. 1998. Updated Nazca (Farallon) – South America relative motions during the last 40 My: implications for mountain building in the central Andean region. *Journal of South American Earth Sciences* **11**(3): 211–215.

Strahler AN. 1952. Hypsometric (area-altitude) analysis of erosional topography. *Geological Society of America Bulletin* **63**(11): 1117ff.

Strecker MR , Alonso R, Bookhagen B, Carrapa B, Hilley GE, Sobel ER, Trauth MH. 2007. Tectonics and climate of the southern central Andes. *Annual Reviews in Earth and Planetary Sciences* **35**: 747–787.

Summerfield MA. 1991. *Global Geomorphology*. Prentice Hall: Englewood Cliffs, NJ; 640 pp.

Thomson SN. 2002. Late Cenozoic geomorphic and tectonic evolution of the Patagonian Andes between latitudes 42 degrees S and 46 degrees S: an appraisal based on fission-track results from the transpressional intra-arc Liquine-Ofqui fault zone. *Geological Society of America Bulletin* **114**(9): 1159–1173.

Tomkin JH, Braun J. 2002. The influence of alpine glaciation on the relief of tectonically active mountain belts. *American Journal of Science* **302**(3): 169–190.

Tomkin JH, Roe GH. 2007. Climate and tectonic controls on glaciated critical-taper orogens. *Earth and Planetary Science Letters* **262**: 385–397.

Tropical Rainfall Measurement Mission (TRMM). 2007. *TRMM*. NASA.

Tucker GE, Slingerland R. 1997. Drainage basin responses to climate change. *Water Resources Research* **33(**8): 2031–2047.

Tucker GE, Bras RL. 1998. Hillslope processes, drainage density, and landscape morphology. *Water Resources Research* **34**(10): 2751–2764.

US Geological Survey (USGS). 2007. *Shuttle Radar Topographic Mission*. USGS: Reston, VA. http://seamless.usgs.gov

Veit H. 1996. Southern Westerlies during the Holocene deduced from geomorphological and pedological studies in the Norte Chico, Northern Chile (27–33°S). *Palaeogeography Palaeoclimatology Palaeoecology* **123**: 107–119.

Vietor T, Echtler H. 2006. Episodic Neogene southward growth of the Andean subduction orogen between 30°S and 40°S – plate motions, mantle flow, climate, and upper-plate structure. In *The Andes – Active Subduction Orogeny. Volume 1: Frontiers in Earth Science Series*, Oncken O, Chong G, Frank G, Giese P, Götze HJ, Ramos VA, Strecker MR, Wigger P (eds). Springer-Verlag: Berlin; 375–400. DOI: 10.1007/978-3-540-48684-8_18.

Whipple K, Tucker GE. 1999. Dynamics of stream-power river incision model: implications for height limits of mountain ranges, landscape response timescales, and research needs. *Journal of Geophysical Research* **104(**B8): 17661–17674.

Whipple KX, Kirby E, Brocklehurst SH. 1999. Geomorphic limits to climate-induced increases in topographic relief. *Nature* **401(**6748): 39–43.

Whipple KX, Meade BJ. 2006. Orogene response to changes in climatic and tectonic forcing. *Earth and Planetary Science Letters* **243**(1–2): 218–228.. DOI. 10.1016/j.epsl.2005.12.022.

Willett SD. 1999. Orogeny and orography: the effects of erosion on the structure of mountain belts. *Journal of Geophysical Research-Solid Earth* **104(**B12): 28957–28981.

Zaprowski BJ, Lal D, Pazzaglia FJ, Evenson EB. 2005. Climatic influence on profile concavity and river incision. *Journal of Geophysical Research – Earth Surface* **110(**F3): F03004.

Zeilinger G, Schlunegger F, Simpson G. 2005. The Oxaya anticline (northern Chile): a buckle enhanced by river incision? *Terra Nova* **17(**4): 368–375.

Appendix

Data repository

Table AI. Correlations between variables: forearc catchments and mountain front catchments

	basin area	basin length	basin width	basin form	basin elongation ration	basin mean elevation	tatal basin relief	basin relief ratio	basin local relief	channel drop	mean annual rainfall	mean annual temperature	ground frost	modern perennial snowline	lowest Pleistocene glaciers	erosion index
Arc																
basin area	1·000															
basin length	0·664* 0·001	1·000														
basin width	0·854** 0·000	0·432 0·045	1·000													
basin form	–0·437 0·042	0·126 0·577	–0·740** 0·000	1·000												
basin elongation ratio	0·052* 0·017	–0·237 0·289	0·591* 0·004	–0·762** 0·000	1·000											
basin mean elevation	–0·190 0·396	–0·071 0·755	–0·111 0·622	0·127 0·572	–0·153 0·496	1·000										
total basin relief	0·009 0·969	–0·166 0·461	0·111 0·623	–0·129 0·567	0·181 0·419	0·816** 0·000	1·000									
basin relief ratio	–0·373 0·087	–0·709** 0·000	–0·201 0·369	–0·195 0·384	0·342 0·120	0·569* 0·006	0·734** 0·000	1·000								
basin local relief	–0·136 0·545	–0·335 0·127	0·061 0·787	–0·266 0·231	0·265 0·233	0·365 0·095	0·526* 0·012	0·587* 0·004	1·000							
channel drop	–0·412 0·057	–0·560* 0·007	–0·328 0·137	0·125 0·578	–0·018 0·938	0·706 0·000	0·726** 0·000	0·829** 0·000	0·448 0·037	1·000						
mean annual rainfall	0·252 0·258	0·316 0·153	0·107 0·634	–0·044 0·846	–0·016 0·942	–0·860** 0·000	–0·855** 0·000	–0·716** 0·000	–0·542* 0·009	–0·850** 0·000	1·000					
mean annual temperature	–0·002 0·991	–0·052 0·818	–0·127 0·573	0·265 0·233	–0·114 0·613	–0·599* 0·003	–0·458 0·032	–0·308 0·163	–0·440 0·040	–0·171 0·445	0·386 0·076	1·000				
ground frost	–0·097 0·668	0·023 0·921	–0·062 0·783	0·038 0·867	–0·095 0·675	0·921** 0·000	0·742** 0·000	0·481 0·023	0·357 0·103	0·546* 0·009	–0·715** 0·000	–0·804** 0·000	1·000			
modern perennial snowline	–0·216 0·333	–0·163 0·468	–0·094 0·676	0·093 0·681	–0·086* 0·704	0·929** 0·000	0·869** 0·000	0·648* 0·001	0·421 0·051	0·795** 0·000	–0·961** 0·000	–0·442 0·039	0·786** 0·000	1·000		
lowest Pleistocene glacier extent	–0·208 0·352	–0·131 0·562	–0·058 0·799	0·078 0·730	–0·108 0·632	0·913** 0·000	0·829** 0·000	0·596* 0·003	0·387 0·075	0·737** 0·000	–0·937** 0·000	–0·438 0·041	0·755** 0·000	0·985** 0·000	1·000	
erosion index	–0·080 0·724	–0·433 0·044	–0·100 0·659	–0·121 0·591	0·187 0·406	0·098 0·664	0·301 0·173	0·442 0·039	0·373 0·087	0·536* 0·010	–0·224 0·316	0·079 0·727	0·105 0·643	0·103 0·649	–0·012 0·957	1·000
erosion intensity	0·804** 0·000	0·336 0·126	0·611* 0·002	–0·383 0·079	0·511* 0·015	–0·440 0·040	–0·156 0·489	–0·307 0·165	–0·139 0·538	–0·323 0·142	0·429 0·046	0·262 0·239	–0·351 0·110	–0·471 0·027	–0·513* 0·015	0·372 0·088

Table AI. *Continued*

	basin area	basin length	basin width	basin form	basin elongation ration	basin mean elevation	tatal basin relief	basin relief ratio	basin local relief	channel drop	mean annual rainfall	mean annual temperature	ground frost	modern perennial snowline	lowest Pleistocene glaciers	erosion index
Subbasins																
basin area	1·000															
basin length	0·397 0·002	1·000														
basin width	0·714** 0·000	–0·006 0·963	1·000													
basin form	–0·406 0·002	0·446 0·001	–0·818** 0·000	1·000												
basin elongation ratio	0·453 0·000	–0·592* 0·000	0·642 0·000	–0·795** 0·000	1·000											
basin mean elevation	–0·496 0·000	–0·393 0·003	–0·149 0·274	–0·011 0·935	–0·042 0·760	1·000										
total basin relief	0·016 0·908	0·112 0·409	0·040 0·768	0·099 0·468	–0·079 0·565	–0·044 0·750	1·000									
basin relief ratio	–0·236 0·080	–0·590* 0·000	0·055 0·688	–0·278 0·038	0·408 0·002	0·147 0·281	0·651* 0·000	1·000								
basin local relief	0·060 0·659	0·008 0·956	0·019 0·889	–0·014 0·920	0·103 0·451	–0·389 0·003	0·537* 0·000	0·485 0·000	1·000							
channel drop	–0·592* 0·000	0·006 0·966	–0·583* 0·000	0·532* 0·000	–0·551* 0·000	0·372 0·005	0·413 0·002	0·225 0·095	0·005 0·973	1·000						
mean annual rainfal	0·519 0·000	0·144 0·290	0·253 0·060	–0·181 0·182	0·273 0·042	–0·829** 0·000	–0·111 0·415	–0·090 0·511	0·411 0·002	–0·551* 0·000	1·000					
mean annual temperature	0·325 0·015	0·353 0·008	0·073 0·591	0·046 0·737	–0·074 0·585	–0·625* 0·000	–0·029 0·831	–0·223 0·098	–0·197 0·146	–0·135 0·320	0·392 0·003	1·000				
ground frost	–0·344 0·009	–0·405 0·002	–0·058 0·672	–0·075 0·583	0·115 0·400	0·748** 0·000	0·016 0·910	0·223 0·098	0·006 0·967	0·165 0·224	–0·515* 0·000	–0·834** 0·000	1·000			
modern perennial snowline	–0·460 0·000	–0·215 0·112	–0·190 0·162	0·114 0·403	–0·183 0·176	0·903** 0·000	0·043 0·751	0·066 0·631	–0·533* 0·000	0·465 0·000	–0·913** 0·000	–0·327 0·014	0·514* 0·000	1·000		
lowest Pleistocene glacier extent	–0·438 0·001	–0·202 0·135	–0·184 0·175	0·106 0·436	–0·189 0·163	0·879** 0·000	–0·008 0·952	0·016 0·908	–0·581* 0·000	0·457 0·000	–0·900** 0·000	–0·277 0·039	0·438 0·001	0·988** 0·000	1·000	
erosion index	–0·284 0·034	0·028 0·838	–0·390 0·003	0·334 0·012	–0·290 0·030	–0·182 0·180	0·303 0·023	0·238 0·078	0·490 0·000	0·575* 0·000	0·196 0·147	–0·127 0·352	0·061 0·655	–0·289 0·031	–0·328 0·014	1·000
erosion intensity	0·579* 0·000	0·274* 0·041	0·246 0·068	–0·094 0·492	0·209 0·122	–0·714** 0·000	0·059 0·665	–0·068 0·618	0·398 0·002	–0·290 0·030	0·819** 0·000	0·320 0·016	–0·420 0·001	–0·778** 0·000	–0·781** 0·000	0·423 0·001

* $R > 0{\cdot}5$.
** $R^2 > 0{\cdot}5$.

Table AII. Correlations between variables: arc catchments and subcatchments

	basin area	basin length	basin width	basin form	basin elongation ratio	basin mean elevation	total basin relief	basin relief ratio	basin local relief	channel drop	mean annual rainfall	mean annual temperature	ground frost	modern perennial snowline	lowest Pleistocene glaciers	erosion index
Forearc																
basin area	1·000															
basin length	0·858** 0·000	1·000														
basin width	0·780** 0·000	0·446 0·043	1·000													
basin form	0·029 0·902	0·446 0·043	–0·0550* 0·010	1·000												
basin elongation ratio	0·081 0·728	–0·385 0·085	0·604* 0·004	–0·869** 0·000	1·000											
basin mean elevation	0·271 0·234	0·439 0·046	0·115 0·620	0·282 0·216	–0·199 0·386	1·000										
total basin relief	0·594* 0·005	0·794** 0·000	0·323 0·153	0·362 0·107	–0·299 0·189	0·817** 0·000	1·000									
basin relief ratio	–0·223 0·331	–0·192 0·405	–0·074 0·749	–0·104 0·654	0·166 0·473	0·688* 0·001	0·417 0·060	1·000								
basin local relief	–0·122 0·598	–0·064 0·784	–0·327 0·148	0·300 0·186	–0·204 0·376	–0·190 0·410	–0·089 0·702	–0·048 0·835	1·000							
channel drop	–0·133 0·564	–0·027 0·909	–0·142 0·540	0·106 0·648	–0·044 0·849	0·784** 0·000	0·507* 0·019	0·888** 0·000	–0·075 0·748	1·000						
mean annual rainfall	–0·509* 0·019	–0·635* 0·002	–0·242 0·290	–0·405 0·068	0·198 0·391	–0·738** 0·000	–0·776** 0·000	–0·363 0·106	0·219 0·341	–0·438 0·047	1·000					
mean annual temperature	0·533* 0·013	0·654* 0·001	0·342 0·129	0·232 0·311	–0·231 0·313	0·647* 0·002	0·659* 0·001	0·148 0·522	–0·455 0·038	0·227 0·322	–0·721** 0·000	1·000				
ground frost	–0·281 0·217	–0·242 0·292	–0·136 0·557	–0·175 0·449	0·084 0·716	0·121 0·600	0·005 0·982	0·301 0·185	0·168 0·466	0·214 0·351	0·399 0·073	–0·375 0·094	1·000			
modern perennial snowline	0·516* 0·017	0·681* 0·001	0·273 0·231	0·353 0·116	–0·240 0·294	0·843** 0·000	0·828** 0·000	0·363 0·105	–0·352 0·118	0·466 0·033	–0·860** 0·000	0·912** 0·000	–0·219 0·340	1·000		
lowest Pleistocene glacier extent	0·443 0·044	0·646* 0·002	0·192 0·404	0·388 0·082	–0·282 0·216	0·865** 0·000	0·840** 0·000	0·419 0·058	–0·311 0·170	0·519* 0·016	–0·846** 0·000	0·878** 0·000	–0·169 0·464	0·993** 0·000	1·000	
erosion index	–0·521* 0·016	–0·523* 0·015	–0·343 0·128	–0·183 0·426	0·100 0·665	0·246 0·282	–0·091 0·696	0·635* 0·002	0·130 0·574	0·727** 0·000	0·250 0·275	–0·329 0·145	0·421 0·058	–0·193 0·403	–0·133 0·567	1·000
erosion intensity	0·252 0·271	0·096 0·678	0·476 0·029	–0·423 0·056	0·320 0·157	0·089 0·702	0·141 0·541	0·085 0·714	–0·058 0·802	0·151 0·514	0·308 0·175	–0·020 0·931	0·358 0·122	–0·039 0·866	–0·052 0·823	0·372 0·097

Table AII. *Continued*

	basin area	basin length	basin width	basin form	basin elongation ratio	basin mean elevation	total basin relief	basin relief ratio	basin local relief	channel drop	mean annual rainfall	mean annual temperature	ground frost	modern perennial snowline	lowest Pleistocene glaciers	erosion index
Mountain front																
basin area	1·000															
basin length	0·515* 0·017	1·000														
basin width	0·984** 0·000	0·522* 0·015	1·000													
basin form	–0·680* 0·001	–0·319 0·159	–0·754** 0·000	1·000												
basin elongation ratio	0·958** 0·000	0·388 0·082	0·959** 0·000	–0·812** 0·000	1·000											
basin mean elevation	–0·074 0·751	–0·075 0·748	–0·135 0·560	0·342 0·129	–0·179 0·438	1·000										
total basin relief	0·185 0·421	0·187 0·416	0·082 0·723	0·282 0·216	0·074 0·748	0·824** 0·000	1·000									
basin relief ratio	–0·300 0·187	–0·706* 0·000	–0·364 0·104	0·431 0·051	–0·270 0·236	0·672* 0·001	0·536* 0·012	1·000								
basin local relief	–0·428 0·053	–0·675* 0·001	–0·445 0·043	0·315 0·165	–0·371 0·098	0·243 0·289	0·081 0·726	0·630* 0·002	1·000							
channel drop	–0·551* 0·010	–0·635* 0·002	–0·595* 0·004	0·640* 0·002	–0·570* 0·007	0·699* 0·000	0·478 0·028	0·896** 0·000	0·605* 0·004	1·000						
mean annual rainfall	0·117 0·612	0·168 0·467	0·189 0·411	–0·328 0·147	0·164 0·476	–0·847** 0·000	–0·811** 0·000	–0·710** 0·000	–0·285 0·210	–0·743** 0·000	1·000					
mean annual temperature	0·018 0·938	–0·222 0·333	–0·039 0·866	0·300 0·187	–0·062 0·789	0·384 0·086	0·371 0·098	0·436 0·048	0·319 0·159	0·502 0·020	–0·456 0·038	1·000				
ground frost	–0·100 0·666	0·139 0·549	–0·125 0·589	0·283 0·214	–0·190 0·409	0·583* 0·006	0·551* 0·010	0·256 0·263	0·147 0·526	0·286 0·209	–0·421 0·057	–0·304 0·180	1·000			
modern perennial snowline	0·059 0·800	0·045 0·846	0·002 0·994	0·220 0·338	–0·035 0·881	0·871** 0·000	0·860** 0·000	0·582* 0·006	0·227 0·322	0·642* 0·002	–0·934** 0·000	0·528* 0·014	0·455 0·038	1·000		
lowest Pleistocene glacier extent	0·131 0·573	0·120 0·603	0·088 0·704	0·113 0·625	0·038 0·869	0·843** 0·000	0·826** 0·000	0·509* 0·018	0·174 0·450	0·562* 0·008	–0·904** 0·000	0·474 0·030	0·443 0·044	0·989** 0·000	1·000	
erosion index	–0·437 0·048	–0·617* 0·003	–0·457 0·037	0·443 0·044	–0·458 0·037	0·478 0·028	0·213 0·354	0·674* 0·001	0·808** 0·000	0·759** 0·000	–0·412 0·064	0·520* 0·016	0·241 0·293	0·430 0·052	0·355 0·114	1·000
erosion intensity	0·897** 0·000	0·436 0·048	0·909** 0·000	–0·614* 0·003	0·849** 0·000	0·025 0·914	0·194 0·398	–0·225 0·326	–0·272 0·232	–0·395 0·076	0·034 0·885	0·181 0·434	–0·051 0·825	0·181 0·432	0·238 0·299	–0·163 0·479

* $R > 0{\cdot}5$.
** $R^2 > 0{\cdot}5$.

Table AIII. Correlations between Hypsometric Integral (HI), Profile Concavity Index (PCI), and morphometric parameters

	Foreac		Mountain Front		Arc		Subbasins	
	HI	PCI	HI	PCI	HI	PCI	HI	PCI
basin area	–0·301	0·042	–0·186	0·225	–0·267	–0·281	–0·469	0·268
	0·185	0·857	0·419	0·326	0·230	0·205	0·000	0·046
basin length	–0·189	0·157	–0·272	0·088	–0·060	–0·014	–0·167	–0·141
	0·411	0·498	0·233	0·706	0·790	0·952	0·218	0·299
basin width	–0·300	0·005	–0·216	0·171	–0·200	–0·379	–0·255	–0·087
	0·187	0·983	0·348	0·459	0·372	0·082	0·058	0·524
basin width	–0·300	0·005	–0·216	0·171	–0·200	–0·379	–0·255	–0·087
	0·187	0·983	0·348	0·459	0·372	0·082	0·058	0·524
basin form	0·155	0·168	0·282	0·031	0·228	0·454	0·151	0·100
	0·502	0·467	0·215	0·895	0·307	0·034	0·267	0·463
basin elongation ratio	–0·113	–0·121	–0·258	0·126	–0·273	–0·318	–0·236	–0·124
	0·624	0·601	0·260	0·585	0·219	0·149	0·079	0·362
basin mean elevation	0·731**	0·828**	0·928**	0·573*	0·980**	0·817**	0·496	0·740**
	0·000	0·000	0·000	0·007	0·000	0·000	0·000	0·000
total basin relief	0·245	0·475	0·590*	0·399	0·717**	0·492	0·175	–0·199
	0·285	0·030	0·005	0·073	0·000	0·020	0·197	0·142
basin relief ratio	0·719**	0·583*	0·683*	0·214	0·503*	0·364	0·165	–0·142
	0·000	0·006	0·001	0·352	0·017	0·096	0·224	0·297
basin local relief	–0·052	–0·383	0·379	–0·355	0·323	0·003	–0·029	–0·508*
	0·823	0·086	0·090	0·115	0·143	0·989	0·835	0·000
channel drop	0·762**	0·587*	0·756**	0·165	0·694*	0·603*	0·522*	0·231
	0·000	0·005	0·000	0·474	0·000	0·003	0·000	0·086
mean annual rainfall	–0·393	–0·595*	0·798**	–0·366	–0·822**	–0·677*	–0·473*	–0·572*
	0·078	0·004	0·000	0·103	0·000	0·001	0·000	0·000
mean annual temperature	0·302	0·671*	0·426	–0·103	–0·534*	–0·382	–0·284	–0·411
	0·184	0·001	0·054	0·657	0·010	0·079	0·034	0·002
ground frost	0·118	0·015	0·462	0·363	0·883**	0·740**	0·266	0·517
	0·612	0·949	0·035	0·105	0·000	0·000	0·048	0·000
modern perennial snowline	0·445	0·758**	0·804**	0·323	0·896**	0·748**	0·465	0·723**
	0·043	0·000	0·000	0·153	0·000	0·000	0·000	0·000
lowest Pleistocene glacier extent	0·481	0·765**	0·785**	0·324	0·881**	0·736**	0·446	0·697*
	0·027	0·000	0·000	0·151	0·000	0·000	0·001	0·000
erosion index	–0·122	–0·624*	0·216	–0·421	–0·181	–0·251	–0·090	–0·453
	0·598	0·003	0·348	0·057	0·421	0·261	0·509	0·000
erosion intensity	–0·562*	–0·680*	–0·571*	–0·759**	–0·567*	–0·537*	–0·494	–0·565*
	0·008	0·001	0·007	0·000	0·006	0·010	0·000	0·000

* $R > 0{\cdot}5$.
** $R^2 > 0{\cdot}5$.